Journal of Arid Environments xxx (xxxx) xxx

Contents lists available at ScienceDirect

Journal of Arid Environments

journal homepage: www.elsevier.com/locate/jaridenv

An open-source approach to characterizing Chihuahuan Desert vegetation communities using object-based image analysis

Andrew R. Bankert [a], Erin H. Strasser [a], Cristy G. Burch [b], Maureen D. Correll [a,*]

[a] Bird Conservancy of the Rockies, Fort Collins, CO, USA
[b] Texas Park and Wildlife, Medard, TX, USA

ARTICLE INFO

Keywords:
Object-based image analysis
Vegetation mapping
Unmanned aerial systems
Grassland vegetation
Automated image analysis
Habitat quantification

ABSTRACT

Methods: for quantifying vegetative cover across landscapes have, until recently, been limited to ground-based surveys or remote sensing via satellites or aircraft, both of which can limit the spatial scale of resulting data. Unmanned Aircraft Systems (UAS) can efficiently collect high-resolution sub-decimeter imagery of landscapes; geographic, object-based image analysis (GEOBIA) of the collected imagery can then be used to estimate vegetation cover. To date, few researchers have utilized open-source programs for GEOBIA. We developed GEOBIA methods in the open-source Program R to analyze visible spectrum UAS imagery from four sites in the Chihuahuan Desert of North America. These desert grasslands are difficult to quantify due to the patchiness of ground cover at small scales (e.g. <1 m) and the rarity of shrubs on the landscape. We used site-specific training data and multiple segmentation parameters to create vegetative and shrub cover data layers at a 15 cm resolution. We report overall accuracies of 77.2%–88.8% for vegetation classification and 95.7%–99.2% for shrub classification. Our work is some of the first to use open-source GEOBIA in grasslands and provides objective, reproducible data layers of desert vegetation, particularly shrubs, at the spatial scale necessary to inform management and conservation of Chihuahuan Desert grassland communities.

1. Introduction

Ecologists often rely on ground-based survey methods to characterize habitat as a component of wildlife monitoring programs. Vegetation structure and composition are important aspects of habitat that often drive differences in demographic vital rates (Halstead et al., 2019), population trends (Hunt et al., 2018), and patterns of habitat use (Shaffer and DeLong, 2019). Rapid-sampling methods (e.g. ocular estimates) to capture information on vegetation cover and height, although widely used in most monitoring protocols, can be imprecise (Godinez-Alvarez et al., 2009), suffer from observer bias, and often only assess small-scale areas. These approaches often miss important information and landscape context, such as the location of an isolated tree or the range of vegetation heights, integral to understanding the mechanistic relationship between habitat and population metrics of interest (Glisson et al., 2015).

Accurate and ecologically representative assessments of vegetation may be particularly challenging in habitats with patchy vegetation (e.g. Huenneke et al., 2001) or during periods of dormancy (Marsett et al., 2006). The grasslands of the Chihuahuan Desert of the southwestern US and northern Mexico are prime examples of such patchy landscapes; these grasslands are characterized by a mosaic of grasses, forbs, and shrubs and interspersed with bare ground. Grazing pressure, soil type, and localized precipitation add to this heterogeneity that varies substantially between years. In particular, shrubs can be difficult to accurately quantify in desert grasslands with rapid ground-based methods because of their low density and spatially variable distribution.

Shrubs, while difficult to quantify, remain an important ecological driver within desert rangelands. Native shrubs such as creosote (*Larrea tridentata*), juniper (*Juniperus),* and mesquite (*Prosopis glandulosa*) are encroaching in Chihuahuan Desert grasslands (Laliberte et al., 2004). This shift can be largely attributed to increasing temperatures and atmospheric CO_2 (Polley et al., 2003), mismanaged grazing, prairie dog declines, and spatial contagion (Bestelmeyer et al., 2018). As the density and composition of shrubs on the landscape changes, wildlife is directly affected by this change. For example, populations of grassland songbirds, an avian group in precipitous decline (−53.2% over 4 decades; Rosenberg et al., 2019), are tightly linked with shrub cover on their wintering grounds. Abundance and winter survival are both negatively associated with increasing shrub cover and height (Macias-Duarte el al.,

* Corresponding author.
E-mail address: Maureen.correll@birdconservancy.org (M.D. Correll).

https://doi.org/10.1016/j.jaridenv.2020.104383
Received 14 April 2020; Received in revised form 25 September 2020; Accepted 30 October 2020
Available online 7 November 2020

2018). Conversely, in young pronghorn (*Antilocapra americana*), survival increases with shrub density on grassland landscapes (Jacques et al., 2015). Shrub encroachment is also one of the driving forces behind grassland loss in the Chihuahuan Desert (Baez and Collins, 2008), and has negative implications for use of these landscapes as rangelands (Anadón et al., 2014).

Recent advances in aerial photography and machine learning can now facilitate the remote sensing of shrubs and other vegetative cover at finer spatial resolutions and over continuous areas much more effectively than traditional surveys. These approaches present a potential cost-effective alternative to ground-based estimation. Although vegetation mapping across very large landscapes (e.g. countries or continents) using satellite imagery has been commonplace for decades (Fuller et al., 1994), these data are often either collected at spatial resolutions too coarse (e.g. 30 m Landsat Operational Land Imager; U.S. Geological Survey, 2016) to capture small objects such as shrubs <0.5 m in diameter or, in the case of finer resolution satellites, under variable sensor and atmospheric conditions giving objects from the same class different spectral properties (Chen et al., 2018). While manned aircraft can collect imagery over large areas at finer resolutions, the high cost and strict regulations often limit the flexibility of this platform for collecting aerial imagery (Chen et al., 2018). Historically, shrubland and grassland ecosystems are particularly challenging to characterize using satellite imagery because of the small footprint of individual species (Lu et al., 2016), large proportion of dead grass (Yang and Guo, 2014), and variable effects of soil reflectance, especially in areas with dead grass (Montandon and Small, 2008). This combination can make these arid lands appear homogeneous in coarser aerial imagery. Monitoring shrub encroachment in desert landscapes using these methods has therefore been challenging, despite a clear need to do so to inform mitigation action in these areas.

Recently there has been significant progress in automated vegetation classification in desert grasslands from imagery collected via Unmanned Aircraft Systems (UAS; Laliberte et al., 2004; Laliberte and Rango, 2011; Dong et al., 2019; Rampant et al., 2019). UAS are increasingly used to characterize vegetation because of their ability to collect fine spatial resolution imagery across both space and time for a relatively low cost (Anderson and Gaston, 2013) and high degree of accuracy (Ma et al., 2017). This imagery can be used to generate data layers including spectral reflectance, surface elevation (digital surface maps, or DSMs), and ground elevation (digital terrain maps, or DTMs) of landscapes with a spatial resolution on the order of centimeters. This level of detail was not previously possible using imagery collected by satellites or manned aircraft. Further processing of these layers can produce unparalleled high-resolution, spatially-explicit data such as canopy height models (Cunliffe et al., 2016), crop maps (Pajares, 2015), biomass estimates (Zhang et al., 2018a), and vegetative cover maps including shrub and grass species (Laliberte and Rango, 2011).

Like any technology, UAS have their share of shortcomings and challenges (see Hassler and Baysal-Gural, 2019). Helicopter-style rotorcraft UAS (e.g. quadcopters, octocopters) have high maneuverability but eat up battery life quickly, limiting the area they are able to survey. Fixed-wing UAS can use less battery life for the amount of area surveyed but lack the positioning accuracy provided using rotorcrafts. All UAS are ultimately limited by the amount of batteries users are able to procure and charge for a day of surveying as well as the weather conditions necessary to successfully collect high-quality imagery. As a result, most studies using UAS technology to quantify vegetative landscapes are limited to smaller areas (e.g. Rampant et al., 2019). Further, there is sometimes a significant initial cost for equipment and time needed to train UAS pilots and familiarize them with the equipment.

Another challenge is the classification of UAS-derived composite imagery into data layers that estimate characteristics of vegetative cover, including shrubs. While pixel-based approaches have traditionally been used to accomplish this (Hussain et al., 2013), a recent paradigm shift towards object-based classification over the past two decades (Blaschke et al., 2014) addresses many of the shortcomings of pixel-based analyses for UAS imagery since pixels are now much smaller than the objects of interest. This method has increasingly been used to efficiently and accurately classify imagery collected via satellite (Robertson and King, 2011), airplane (Laliberte et al., 2004) and UAS (Dong et al., 2019). This approach, also referred to as GEOBIA, divides remotely sensed imagery into clusters of similar pixels (called objects) in a process called segmentation, and then evaluates the characteristics of each object (Hay and Castilla, 2008). This approach can also quantify contextual properties, such as object shape, size, and texture, in addition to spectral and geographical properties, which better represents how the human eye and brain analyze images (Blaschke et al., 2014). Segmentation can be completed using several types of algorithms including pixel-based, edge-based, and region-based approaches, with the latter being further divided into region-growing, region-splitting, and region-merging techniques (Blaschke et al., 2004). Region-growing is currently the most widely applied segmentation algorithm due to its success in a variety of settings and data sources (Ma et al., 2017). It is also possible to hone the spatial scale at which segments are identified using scale parameterization, although this optimization step does not always result in higher classification accuracies (Chen et al., 2018). The identified segments can then be classified into categories of cover based on the properties of the individual segments using a variety of approaches (e.g. Random Forests, Classification and Regression Trees; Li et al., 2016).

These GEOBIA techniques often outperform pixel-based approaches in cases where the pixels are smaller than the objects of interest (e.g. Hussain et al., 2013). Even in cases of comparable classification accuracies between GEOBIA and pixel-based methods (Robertson and King, 2011), object-based classification often produces more realistic results by returning fewer illogical errors and avoiding the 'salt and pepper effect' of pixels of multiple incorrect classes interspersed in a small area (Blaschke et al., 2010). Object-based analysis of remotely sensed imagery is usually (>85%) completed using proprietary software (Ma et al., 2017), which can add expenses and limit flexibility in image segmentation or use on projects with limited budgets. Open-source software can reduce cost and also increase customizability for object-based analyses; several open-source applications of GEOBIA exist including Orfeo Toolbox (e.g. Deluca et al., 2019), open python script (e.g. Clewley et al., 2014), and Spring (e.g. Teodoro and Araujo, 2016). However, to date no GEOBIA methods have been designed in Program R, the open-source programming language most widely used in ecological data analysis (Lai et al., 2019).

We used GEOBIA techniques to create a program to classify shrub and other vegetative cover at several large (>500 ha) desert grassland sites in the Chihuahuan Desert with UAS-derived imagery and open-source software (Program R) familiar to ecologists. These sites were part of a regional study to understand limiting factors for winter survival of grassland birds. Our objective was to create a user-friendly approach to input a set of training data and UAS-generated maps to measure shrubs on the landscape as well as create accurate land cover maps (>70% overall accuracy) for future use in ecological modeling of desert grassland landscapes. We used hierarchical, object-based classification techniques to successfully create maps showing the cover type, location of shrubs, and object heights across large desert landscapes. We also developed and applied a hybrid classification approach for a subset of these cover types using pixel-based approaches to accurately reflect spatial heterogeneity on the landscape. All of our developed code is accessible through GitHub at https://github.com/andy-bankert/GEOBIA-in-R. These methods and resulting layers can be used by ecologists to understand vegetation composition and context landscape within the Chihuahuan Desert.

2. Methods

2.1. Study sites

We collected imagery and classified vegetation at four ecologically distinct grassland/shrubland sites in the Chihuahuan Desert (Fig. 1). The Chihuahuan Desert is a diverse ecoregion with elevation ranging.

from 600 to 1800 m above sea level characterized by temperatures that can reach freezing or exceed >50 °C. Most of the region's precipitation, an average of 235 mm annually, occurs during localized late-summer monsoons, and some precipitation occurs in the form of snowfall during the winter. Our sites were on private, working rangelands within Grassland Priority Conservation Areas (GPCAs). One study site was located in the Cuchillas de la Zarca GPCA in Durango, Mexico and consisted of three distinct polygons totaling 724 ha at an average elevation of 1800 m (hereafter the Durango site). Vegetation at this site was characterized by grasses in the genera *Aristida*, *Bouteloua*, *Muhlenbergia*, *Panicum,* and *Bothriochloa* and shrubs within the genera *Juniperus, Acacia,* and *Prosopsis.* The second site was at an average elevation of 1400 m within the Janos GPCA in the state of Chihuahua, Mexico and was 999 ha (hereafter the Chihuahua site). This site was characterized by grasses of the genera *Aristida*, *Bouteloua*, *Eragrostis*, *Panicum, Pleuraphis,* and *Bothriochloa* and shrub species *Ephedra trifurca* and *Prosopis glandulosa*. Invasive Russian thistle (tumbleweed, *Salsola spp.)* was ubiquitous in some years, and kangaroo rat (*Dipodomys spp.*) mounds are scattered throughout the site. Our third study site was located in the Marfa GPCA in Texas, USA consisting of two plots totaling 720 ha at an average elevation of 1400 m (hereafter the Texas site). One plot was within a continually grazed pasture and the other was in a rotationally grazed pasture. This site was dominated by grasses in the genera *Bouteloua* and *Aristida*, with shrubs in the genera *Prosopsis* and *Yucca*, although shrub cover was very limited at this site. Our fourth study site was a valley grassland located in the Valle Colombia GPCA in Coahuila, Mexico and consisted two plots totaling 627 ha at an average elevation around 1200 m (hereafter the Coahuila site). This study area was dominated by grasses in the genera *Bouteloua, Hilaria,* and *Aristida*, with and shrubs in the genera *Prosopsis* and *Yucca*, although shrub cover was also very limited at this site. All sites were grazed by domestic cattle (*Bos taurus*) and/or bison (*Bison bison*).

3. Field data collection

We flew a Sensefly eBee Plus (Sensefly, Cheseaux-Lausanne, Switzerland) fixed-wing UAS with a SenseFly S.O.D.A. 1" RGB sensor with an f/2.8–11, 10.6 mm, and 20 Megapixel resolution lens over our study sites in December 2017–March 2018 to collect aerial imagery representative of winter conditions at each site. We developed a flight plan for each site using eMotion software (Sensefly, Cheseaux-Lausanne, Switzerland) to fly transects ~120 m above ground level oriented perpendicular to the wind and capture images with a 2–3 cm resolution and with a 70–75% horizontal and vertical overlap as recommended by Pix4d to produce DSMs, DTMs, as well as orthomosaics (Pix4d version 4.3.31, Prilly, Switzerland). Where possible we extended these flights beyond the study site boundaries to ensure optimal image overlap ($n \geq 5$) necessary for 3D-surface estimation. We flew the UAS when weather conditions were mostly clear (<10% cloud cover) or completely overcast and attempted to collect data within 3 h of solar noon to avoid large shadows associated with a low sun angle and partly cloudy skies. We did not fly when winds exceeded 46 km/h to avoid damaging the UAS.

We also identified and recorded information for ground control points (GCPs) on highly visible, stationary objects (e.g. wooden posts, cattle guards, water tanks, large rocks) throughout our study sites (Appendix A) using a Trimble Geo7 GTX GPS (Trimble, Sunnyvale, California). Since we did not always have access to a high-accuracy GPS at the same time we collected the imagery and were not given permission to leave large targets on working ranches, we did not use black and white targets commonly used to ground reference aerial imagery. We photographed and took detailed notes on the GPS unit location in order to accurately relate the location of each the GPS point to individual pixels in the UAS imagery. We collected between 6 and 34 GCPs at each study site depending on the total area of the site, number of distinct polygons within a site, and the availability of suitable objects.

4. Raster creation

We used the photogrammetry software Pix4D Mapper (Pix4d, 2017) to process collected imagery to produce a DSM, DTM, and orthomosaic map of each study site. Pix4d uses photogrammetry to create a point cloud of elevation data which can then be processed to create elevation surfaces. Previous work has reported a mean vertical deviation of 8 cm (SD = 8 cm) in Pix4d point clouds in grasslands (Zhang et al., 2018b),

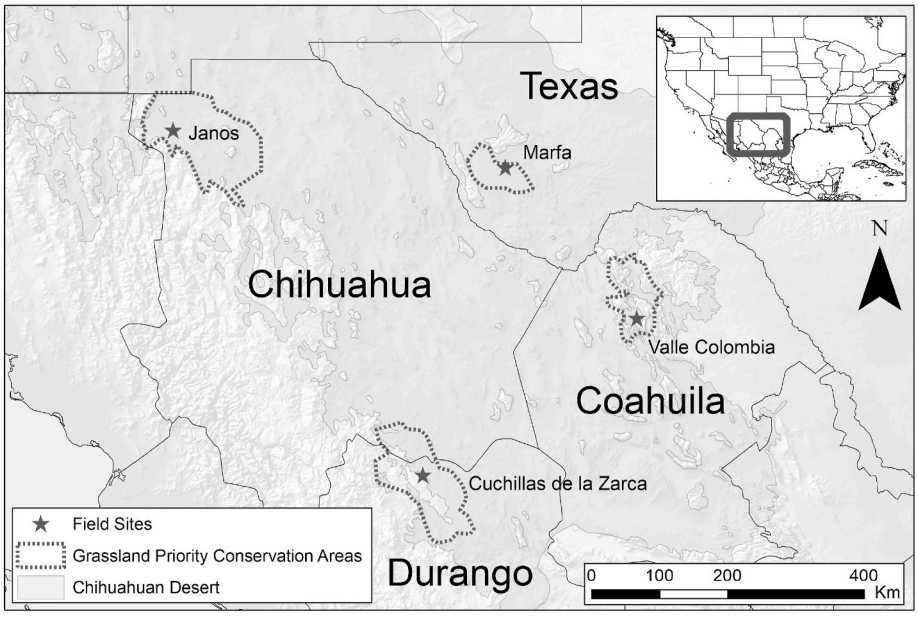

Fig. 1. A map of four grassland bird winter survival monitoring sites and Grassland Priority Conservation Areas in the Chihuahuan desert.

which falls well under the threshold we use for our prominence parameter (15–30 cm; see Fig. 2) and crown height cutoff (30 cm). We first used Pix4D to stitch together aerial photographs and generate a sparse point cloud using the software's structure-from-motion algorithms. After initial processing, we added GCPs collected in the field to georeference the point cloud. The root mean square error for GCPs reported by Pix4d ranged from 0.2 to 1.1 m. We ran Pix4d's 'Reoptimize' step to incorporate the ground control points into the point cloud. With the ground control points incorporated, we created a dense point cloud as an intermediary step before running Pix4d's final step creating our final rasters for analysis. To optimize processing time we ran the dense point cloud on the 'low' setting which calculated approximately 40 points/sq. m, and the Pix4D software classified the point cloud so it could produce the DTM by creating a contour map based on points classified as ground points. We maintained the spatial resolution of the orthomosaic and DSM at the same resolution of the drone imagery (~2–3 cm) and set the spatial resolution of the DTM to 25x the resolution of the DSM (~75 cm) to minimize effects of areas where Pix4D misclassified vegetation as ground points. Since the study sites generally had mild sloping topography, extra detail from a DTM with a pixel size <75 cm was not necessary.

5. Training data collection

Supervised classification models require training to describe the characteristics of cover types to be classified within the available imagery. Because each study site was ecologically distinct, we collected training data specific to each study site. At each site we first determined the cover types relevant for the area (Table 1). Technicians familiar with local study-site characteristics then digitized polygons of these cover types on 13–20 (depending on site area and ecology; Appendix B) 100 m × 100 m orthomosaic tiles within each study site that contained these cover types (Fig. 2). Our goal was to create 100–400 polygons for each cover type to incorporate a wide variety of polygons for each cover type without unnecessarily creating an excessive number of polygons. However, in some cases we created <100 polygons for uncommon cover types (e.g. *Opuntia*) and >400 polygons for cover types with similar spectral characteristics to other cover types (e.g. small shrubs with similar spectral characteristics to grass) to increase classification accuracy.

6. Automated vegetation classification

We created a two-phase, automated process to create vegetative cover data layers of our study site using the resulting DTMs, DSMs, and orthomosaics with Program R with the general outline shown in Fig. 3. Both phases initially segmented the study site into objects using a region-growing technique and then assigned spectral and spatial features (e.g. color, hue, and elevation) to each object. The first phase used the features and assigned cover type for each object in the training dataset to build a random forest (RF) model, and the second phase used this RF model to assign a cover type to every object in the study site. RF models create a large number of unique decision trees based on object properties from training data, and each decision tree in the 'forest' independently determines a classification for an object and all the decision trees vote on the object's final classification. The objects gets classified as the class that gets the most votes from the forest of decision trees.

Prior to image segmentation we compiled the DSM and DTM elevations and the three orthomosaic color bands (red, green, and blue; RGB) within 100 m × 100 m tiles into a set of stacked rasters to eventually create 12 data layers (Table 2). This tile-by-tile analysis allowed us to analyze multiple tiles in parallel to increase efficiency during processing. We scaled all color rasters to values between 0 and 1 to simplify calculating other color properties such as intensity, hue, and saturation. We derived an additional seven data layers for use in our classification effort based on these inputs. We used the DTM and DSM rasters to derive 1) slope at each pixel, 2) relative elevation for each pixel (DSM-DTM, setting values to zero), and 3) a binary 'probable shrub' layer identifying pixels above and below the prominence parameter. We considered relative elevation to be erroneous when the elevation of the DTM was above the DSM, since the surface elevation cannot be below the ground elevation, and when the relative elevation was >100 m since we do not have any cases of objects with >100 m prominence at our study sites.

Table 1
Vegetation cover types at four grassland study sites across the Chihuahuan Desert. Cover types listed in bold are considered shrubs.

Durango	Chihuahua	Texas	Coahuila
–	*Amaranth*	–	–
Bare Ground	Bare Ground	Bare Ground	Bare Ground
Brickellia	***Ephedra***	-	*Hilaria*
Grass	Grass	Grass	Grass
Juniperus	*Dipodomys* mound	–	*Opuntia*
–	***Prosopis***	-	***Prosopis***
Other Shrub	**Other Shrub**	**Other Shrub**	**Other Shrub**
–	Rocks	–	–
Shadow	Shadow	Shadow	Shadow
–	*Pleuraphis*	–	–
–	*Salsola*	*Salsola*	–
Yucca	***Yucca***	***Yucca***	***Yucca***

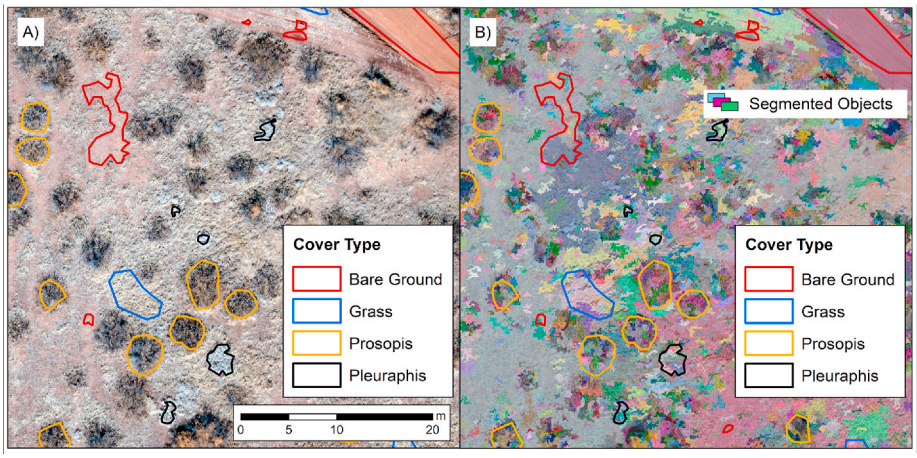

Fig. 2. Examples of A) a sample training area with digitized polygons and B) a raster with object IDs after initial segmentation overlaid onto aerial imagery collected in desert grasslands near Janos, Chihuahua, MX.

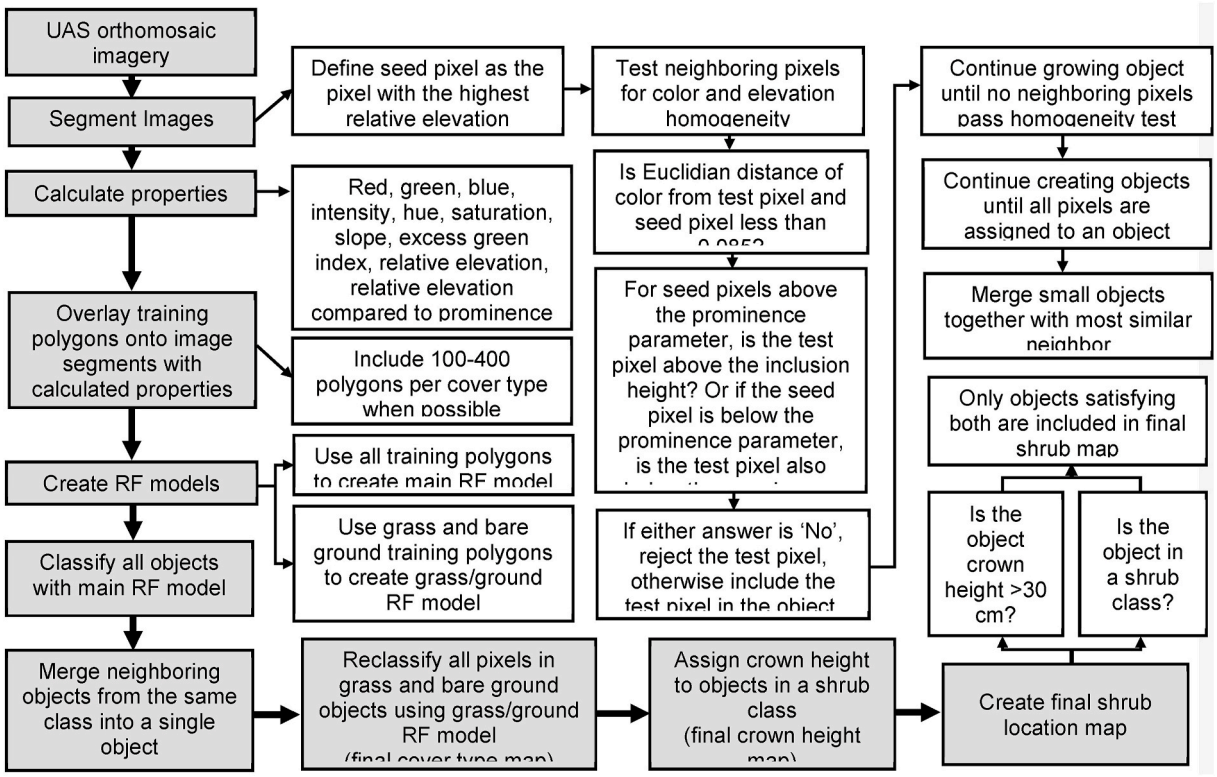

Fig. 3. A schematic of the automated vegetation classification program that converted UAS imagery into cover type maps.

Most erroneous relative elevation points were either small negative values scattered throughout the study site or excessively large values at the edge of the imagery where the DSM and DTM were built with fewer images. We used the RGB color bands to derive: 4) intensity (the total amount of light reflected), 5) hue (the dominant color), 6) saturation (the pureness of the color), and 7) the Excess Green Index (ExG; 2G – R – B; Meyer et al., 1994). This effort created a total of 12 data layers for use in image classifications.

We build in four input parameters to the segmentation and classification process to allow for flexibility in study site segmentation: 1) pixel resolution, 2) prominence parameter, 3) minimum object size, and 4) inclusion height. We used a 15 cm resolution at all study sites to process our large study sites in a reasonable time while still capturing multiple pixels on each individual shrub. We set the prominence parameter (Fig. 4) depending on local vegetation ecology. At sites with clearly defined large shrubs (Chihuahua and Durango) we used a 30 cm prominence parameter, and at sites where most of the vegetation was short (Coahuila and Texas) we used a 15 cm prominence parameter. These values provided the most accurate results for isolating small

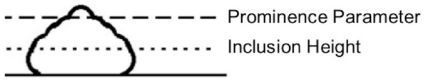

Fig. 4. A schematic of a shrub describing 1) prominence parameter (dashed line), and 2) inclusion height (solid line), both model parameters included in a classification of vegetative cover in the Chihuahuan Desert.

shrubs from grass and bare ground during the image segmentation process. The prominence parameter served only as a tool for segmenting objects that rose above the ground level at each study site, especially isolating small shrubs from similar looking patches of grass. This parameter did not limit which cover types existed above or below the chosen height. We defined the minimum object size as 0.25 m^2, or the area of a small shrub. This allowed us to identify small shrubs but prevented segmentation into objects smaller than shrubs (e.g. a small hole or an isolated small rock). Objects below this threshold merged into the most similar neighboring object. We set the inclusion height to 50% of the prominence parameter height (Fig. 4) to include lower-lying pixels

Table 2
Definitions of data layers generated from UAS imagery used to classify objects into cover types.

Variable	Description
Red	Amount of red reflected on a pixel (scaled from 0 to 1)
Green	Amount of green grflectreen on a pixel (scaled from 0 to 1)
Blue	Amount of blue blflectlue on a pixel (scaled from 0 to 1)
DSM	Surface elevation of a pixel above sea level (m)
DTM	Ground elevation of a pixel above sea level (m)
Slope	Difference in ground elevations of all 8 surrounding pixels with neighboring pixels weighted higher than diagonal pixels (Horn, 1981; radians)
Relative Elevation	Difference between surface elevation and ground elevation at a pixel (m)
Binary 'Probable Shrub'	Is a pixel's relative elevation above the prominence parameter? (1 = yes, 0 = no)
Intensity	Total amount of light reflected at a pixel (scaled from 0 to 1)
Hue	Dominant color of a pixel on a color wheel (0–359)
Saturation	Pureness of the color at a pixel (scaled from 0 to 1)
Excess Green Index	2*Green - Red - Blue (Meyer et al., 1994)

with objects containing pixels above the prominence parameter.

7. Image segmentation and feature selection

We first segmented images by grouping pixels into discrete objects by evaluating color and elevation properties. We used an iterative region-growing process to segment tiles. We first selected a seed pixel and then tested neighboring pixels for elevation and color homogeneity in a nested loop that grew the object. We defined the seed pixel as the pixel with the highest relative elevation not already assigned to an object. For the first nested loop iteration, the model tested all eight neighboring pixels, including diagonally adjacent pixels, for homogeneity by: 1) calculating the Euclidian distance (Equation (1)) from the three color bands of the seed pixel to the color bands of the test pixel, and 2) assessing the relationships of the seed pixel to the prominence parameter and the test pixel to the inclusion height parameter. To only include pixels with similar colors in each object, we rejected test pixels with a Euclidian distance of the color bands >0.085 from the seed pixel. We also tested the model using the Euclidian distance in the intensity-hue-saturation color space, but we only used the RGB color space to determine homogeneity to reduce model complexity. For seed pixels above the prominence parameter, we rejected test pixels below the inclusion height parameter, and for seed pixels below the prominence parameter we only accepted test pixels below the prominence parameter. We grouped test pixels that passed both the color test and the relative elevation test into the object. For subsequent loops, we only evaluated untested adjacent, but not diagonal, neighboring pixels to avoid checkerboard patterned objects. Each successive loop grew the object until no neighboring pixels passed both homogeneity tests, thus finalizing the object. We continued creating objects until the model assigned each pixel on the tile to an object (Fig. 2).

We merged objects below the minimum object size threshold into neighboring objects with the most similar properties. We gave priority to neighboring objects that had pixels with relative elevations on the same side of the prominence parameter, and then picked a best match for the object based on the smallest Euclidian distance between the averages of each RGB color band. We assigned features to each object created during the image segmentation including mean reflectance value for RGB bands, intensity, hue, saturation, ExG, and relative elevation. We also included the 95th percentile relative elevation as an estimate of object crown height, the percentage of pixels above the prominence parameter, the maximum slope, and total area. We included the maximum slope as a feature since many shrubs rise steeply above gentle sloping grasslands, giving many shrub objects a higher maximum slope than non-shrub objects.

8. Random forest creation and object classification

To create property signatures to use for object classification, we developed an RF model by overlaying collected training data polygons on segmented 100 m × 100 m tiles. We built a list of computer-segmented objects for each cover type by including all objects with ≥60% overlap to the hand-drawn training data polygons. Since our program tended to over-segment images, each hand-drawn polygon often had multiple computer-segmented objects. We chose 60% as the cutoff value to avoid including polygons of the majority wrong class in the training process while still including polygons on the edge of objects. For cover types represented by large, continuous objects (i.e. combined bare ground and grass cover), we included any object overlapping the training data polygon that included ≥5 pixels of the cover type and contained more pixels in that cover type than in any other training polygon. We used the R package 'randomForest' (Liaw and Weiner, 2002) to create a RF model with our training dataset. We set the number of features to test at each node (mtry) to 10 and the number of decision trees (ntree) to 4000. These mtry and ntree values produced the lowest out-of-bag error, which determines how well a RF model fits a dataset, at the Chihuahua study site (Appendix C).

We also created a pixel-based RF model to further separate grass pixels and bare ground pixels in objects classified as either grass or bare ground. Since both grass and bare ground at our study sites typically doesn't form well-defined objects and are often mixed together at scales similar to or finer than our analysis pixels (0.02 m^2), we used this hybrid approach to classify grass and bare ground cover types. We used the features associated with pixels enclosed by grass and bare ground training polygons to create the pixel-based RF model (mtry = 2, ntree = 2000). These mtry and ntree values also produced the lowest out-of-bag error at the Chihuahua study site (Appendix C).

We used the object-based RF model to classify each object in each study site. After classifying each object, we merged all neighboring objects with the same cover type into a larger object of that class. For example, a cluster of neighboring objects classified as *Yucca* were merged into a single object classified as *Yucca*. We used the pixel-based RF model for objects classified as grass or bare ground to reassign each pixel within these objects to either grass or bare ground. We calculated the 95th percentile relative elevation using the DSM raster within each shrub object and used these values to create a crown height layer. Finally, we created a binary shrub layer for each study site by combining all objects that: 1) were classified as a shrub cover type, and 2) had a crown height >30 cm. We chose a 30 cm crown height to match field-based data collection protocols used at these sites, and this value was independent of the prominence parameter.

Due to the ecological complexity of the Chihuahua study site, we developed systematic corrections to our layers based on our knowledge of the area for regularly misclassified objects for this site. Specifically, a visual inspection of the results revealed that *Pleuraphis spp.* grass patches (a genera localized at the Chihuahua study site) were consistently misidentified as other shrubs due to their spectral similarity to other shrubs at the Chihuahua site. Because most objects correctly classified as other shrubs had >15 cm relative elevation and almost all *Pleuraphis* patches had <15 cm relative elevations, we reclassified any other shrub object with a crown height <15 cm as *Pleuraphis*. Dark patches of grass inside large areas of *Pleuraphis* were also consistently misclassified as *Prosopis* because of their similar color and area. We therefore reclassified any *Prosopis* objects with a crown height <12 cm as grass since *Prosopis* shorter than 12 cm were almost nonexistent at the Chihuahua site.

9. Accuracy assessment

We calculated classification accuracy by measuring the area correctly classified within each derived layer when compared with photo-interpreted validation data. To collect validation data we digitized a portion of the study area using similar procedures to training data collection. We randomly selected 100 tiles across each study site and then created a 10 × 10 m square area near the center of each tile to digitize as validation data. Many areas within the study sites have both grass and bare ground within small areas (<0.25 m^2) that we could not isolate when digitizing; in this case we used a sparse grass cover type to represent ground with bare ground and short, sparse grass mixed together during validation only. We also used an unknown cover type for regions where we could not identify the cover type in our validation tiles.

We summed the number of pixels correctly classified within each validation cover-type polygon and divided by the total number of pixels within the polygon to calculate the overall classification accuracy. For areas digitized as sparse grass, we considered both grass and bare ground as correct classifications. We omitted pixels either digitized or classified as shadow because we could not determine the true cover type and we also omitted pixels digitized as unknown. We calculated a separate shrub classification accuracy by comparing the number of pixels correctly identified as either a shrub or a non-shrub cover type to the total number of pixels within the validation polygons. For the shrub classification accuracy, a *Juniperus* pixel classified as *Prosopis* was

counted as correctly identified as a shrub, and a grass pixel classified as bare ground was also counted as correctly identified as a non-shrub. We calculated the producer's accuracy by dividing the number of pixels correctly classified by the number of pixels of that class identified during the validation process, and we calculated the user's accuracy by dividing the number of correctly verified pixels by the number of pixels classified by the computer for a given class. These measurements calculated the accuracy by percentage of area correctly identified.

We also measured the quantity and allocation disagreement based on Pontius and Millones (2011), an object location accuracy, and a segmentation factor. The allocation disagreement compares the configuration of reference and classified maps, and the quantity disagreement compares the percentage of each class between a reference and classified map. Since calculating quantity and allocation disagreement requires the same number of rows and columns in the confusion matrix, we combined bare ground, grass, and sparse grass into a single class since we created a separate category (sparse grass) for regions where we could not always reliably separate bare ground from grass. We measured the object location accuracy by calculating the percentage of verification polygons where the computer correctly identified at least one pixel within the digitized polygon. This form of assessment measures how well the computer located certain objects rather than how well it delineated them. For some cover types with <50% producer's classification accuracy (*Dipodomys* mounds, *Ephedra*, and *Salsola*) at the Chihuahua site we created an additional 100 polygons in randomly selected areas to supplement verification polygons so we could more robustly assess how well our model located these cover types. This measurement calculated the accuracy by dividing the number of validation polygons correctly identified by the total number of validation polygons for the class. Since many of the shrubs at the study sites displayed a wide variation in spectral patterns, the image segmentation process tended to oversegment shrubs. We quantified this oversegmentation factor by counting the number of objects within shrub training polygons and dividing by the number of training polygons for the particular shrub class to get an average number of object segments per training polygon. This factor only measured the accuracy of the image segmentation step and not the classification step, and if multiple objects within a polygon were classified to the correct class this assessment still counted each object separately when determining the oversegmentation factor.

10. Results

Overall classification accuracies ranged from 77.2% to 88.8% and shrub classification accuracies from 95.7% to 99.2% across four study sites (Table 3). We also present the confusion matrix for all cover types at each study site in Tables 4–7. We present object location assessments for all study sites in Table 8. We correctly assigned sparse grass, or areas with mixed grass and bare ground, to either grass or bare ground with high (92.7%–99.8%) accuracy across each study site.

At the Durango study site, we found 77.2% overall classification accuracy and 95.7% shrub classification accuracy (Table 4). Two of the five individual cover types (*Juniperus* and other shrub) had producer's accuracies >70% and grass and *Juniperus* had user's accuracies >70%.

Table 3
Overall vegetation classification and shrub classification accuracies of an object-based RF classification model at four grassland sites across the Chihuahuan Desert.

Site	Overall Classification	Shrub Classification
Durango	77.2%	95.7%
Chihuahua	79.0%	97.2%
Texas	88.8%	99.8%
Coahuila	86.9%	98.1%

Bare ground had a particularly low classification accuracy (<40% for producer's and user's accuracies). Of these misclassified pixels, 67.1% came from a paved highway where the UAS imagery appeared darker in validation polygons along the highway in the northwestern part of the study area when compared to the same highway in the training polygons from the southeastern part of the study area. The model classified 63.3% of the misclassified bare ground pixels as grass, and it classified 90.6% of the incorrectly classified grass pixels as bare ground. Only two of the five cover types, bare ground (74.9%) and *Brickellia* (47.0%) had <85% producer's shrub classification accuracy. Other shrub (58.4%) and *Brickellia* (32.0%) were the only classes with <85% user's accuracy. The quantity disagreement was 2.6% and the allocation disagreement was 1.9%. The model correctly located 93.6% of the other shrub, 98.6% of the *Juniperus*, and 63.8% of the *Brickellia* objects for the object location accuracy (Table 8).

At the Chihuahua site we found 79.0% overall classification accuracy and 97.2% shrub classification accuracy (Table 5). The model correctly classified five (bare ground, grass, *Prosopis*, *Pleuraphis*, and *Yucca*) of the eight cover types encountered in the verification tiles with >70% producer's accuracy and three cover types (bare ground, grass and *Pleuraphis*) with >70% user's accuracy. Producer's shrub classification accuracy was >70% for each cover type with the exception of *Ephedra* (65%) and user's shrub class accuracy was >70% for each cover type except *Ephedra* and *Prosopis*. The quantity disagreement was 2.4% and the allocation disagreement was 8.8%. The object location accuracy was >70% for most cover types, with only *Salsola* (69%) and *Ephedra* (59%) having <70% of verification polygons with at least some pixels belonging to the correct cover type (Table 8).

At the Texas site we found 88.8% overall classification accuracy and 99.8% shrub classification accuracy (Table 6). The model correctly classified grass (78.4%) and bare ground (80.2%) with >70% producer's accuracy and only grass (99.1%) with >70% user's accuracy. Two of the three shrub cover types (other shrub and *Yucca*) had between 60% and 70% producer's accuracy and Yucca had a 65.5% user's accuracy while other shrub had 46.5% user's accuracy. The model did not correctly identify any *Salsola*, which only represented 0.02% of validation pixels, during the verification process. Other than other shrub (66.9% producer's and 59.7% user's) and *Yucca* (83.6% producer's and 72.9% user's), the model correctly predicted the shrub classification accuracy of the remaining cover types at >90%. The quantity disagreement was 0.1% and the allocation disagreement was 0.2%. The object location accuracy was 73.1% for other shrubs and 84.6% for *Yucca* (Table 8).

At the Coahuila study site, we found 85.7% overall classification accuracy and 98.0% shrub classification accuracy (Table 7). We found class-level producer's accuracies >70% for three cover types (bare ground, grass, and other shrub) and 65–70% class accuracies for *Hilaria* and *Yucca* with >70% user's accuracies for three cover types (bare ground, grass, and *Yucca*). The shrub classification producer's accuracies for 5 of the cover types was >85% with only the *Prosopis* (53.1%) and *Opuntia* (55.6%) cover types with <85% shrub classification accuracy. The shrub classification user's accuracies were >80% for *Hilaria*, grass, bare ground, and *Yucca* with *Prosopis* (29.8%) and other shrub (59.5%) showing lower shrub classification user's accuracies. The quantity disagreement was 2.7% and the allocation disagreement was 3.8%. The object location accuracy was 90.9% for *Hilaria* patches, 79.6% for *Prosopis*, 100% for other shrubs, and 83.3% for *Yucca* objects (Table 8).

The results of the oversegmentation factor are shown in Table 9. The oversegmentation factor varied between 1.8 and 40.4 with an average value of 11.8 and a median value of 6.7. The program showed the highest number of objects in the classes with the largest training polygons (*Juniperus* at the Durango site and *Prosopis* at the Chihuahua site).

11. Discussion

Vegetative cover assessment of UAS-derived imagery can create

Table 4
Confusion matrix showing the number of pixels in verification areas at the Cuchillas de la Zarca Grassland Priority Conservation Area in Durango, MX. Bold numbers refer to pixels where both the model and hand verification identified the same cover type. The accuracies reported show both the percentage of pixels assigned to the correct cover type and the percentage of pixels where the model correctly determined whether the pixel belonged to a shrub or a non-shrub.

	Bare Ground	Grass	*Brickellia*	*Juniperus*	Other Shrub	Sparse Grass[a]	Unknown[b]	Shadow[b]
Bare Ground	**3564**	65963	370	192	509	**39163**	3287	1369
Grass	4868	**151969**	938	241	891	**73351**	5960	2613
Brickellia	51	2604	**1034**	508	139	913	722	127
Juniperus	87	2774	115	**22494**	316	931	376	1132
Other Shrub	2685	1475	9	45	**8409**	1869	1449	423
Shadow	1282	5770	243	2528	1111	4863	1675	30622
Producer Class Accuracy	31.7%	67.6%	41.9%	95.8%	81.9%	96.8%	–	–
Producer Shrub Accuracy[c]	74.9%	97.0%	47.0%	98.2%	86.4%	96.8%	–	–
User Class Accuracy	38.9%	97.0%	19.7%	84.2%	58.0%	–	–	–
User Shrub Accuracyc[c]	99.0%	99.1%	32.0%	85.8%	58.4%	–	–	–
% Overall Correct Cover Type	77.2%	–	–	–	–	–	–	–
% Overall Correct Shrub Classification	95.7%	–	–	–	–	–	–	–
Quantity Disagreement	2.6%	–	–	–	–	–	–	–
Allocation Disagreement	1.9%	–	–	–	–	–	–	–

[a] Pixels in the Sparse Grass cover type were considered correct if the model predicted either Bare Ground or Grass.
[b] The accuracy of Unknown and Shadow were not included in error assessment.
[c] We considered *Brickellia*, *Juniperus*, Other Shrub, and *Yucca* as shrubs; we considered all other cover types as non-shrubs except Shadow.

Table 5
Confusion matrix showing the number of pixels in verified areas at the Janos Grassland Priority Conservation Area in Chihuahua, MX. Bold numbers refer to pixels where both the model and hand verification identified the same cover type. The accuracies reported show both the percentage of pixels assigned to the correct cover type and the percentage of pixels where the model correctly determined whether the pixel belonged to a shrub or a non-shrub.

	Bare Ground	*Ephedra*	Grass	*Dipodomys* mound	*Prosopis*	Spare Grass[a]	*Pleuraphis*	*Salsola*	*Yucca*	Unknown[b]	Shadow[b]
Amaranth	0	0	254	0	0	0	0	89	0	9	0
Bare Ground	**35513**	98	37984	1103	615	**82539**	5515	1301	4	681	313
Ephedra	3	**888**	917	0	452	266	82	273	89	656	216
Grass	6743	382	**124063**	329	1984	**70322**	10460	4833	33	2307	1037
Dipodomys mound	885	9	570	**1113**	39	2440	0	66	0	68	80
Prosopis	249	253	2772	6	**10308**	2309	293	1503	23	971	1120
Rocks	3	0	0	0	85	28	0	0	0	0	12
Pleuraphis	904	9	4518	0	7	3829	**48500**	5	17	402	157
Salsola	50	137	1695	9	1045	724	7	**7063**	10	768	150
Yucca	13	49	0	0	1	171	0	0	**476**	3	47
Other Shrub	323	0	6	0	0	2241	55	0	9	309	4
Shadow	148	81	255	5	503	423	119	123	19	100	1756
Producer Class Accuracy	79.5%	48.7%	71.8%	43.5%	70.9%	92.7%	74.7%	46.7%	72.0%	–	–
Producer Shrub Accuracy[c]	98.7%	65.2%	97.9%	99.8%	74.0%	97.0%	99.3%	88.3%	90.3%	–	–
User Class Accuracy	71.7%	29.9%	88.7%	21.7%	58.2%	–	83.9%	65.8%	67.0%	–	–
User Shrub Accuracy[c]	99.6%	48.1%	98.9%	99.1%	59.7%	–	99.9%	88.9%	74.1%	–	–
% Overall Correct Cover Type	79.0%	–	–	–	–	–	–	–	–	–	–
% Overall Correct Shrub Classification	97.2%	–	–	–	–	–	–	–	–	–	–
Quantity Disagreement	2.4%	–	–	–	–	–	–	–	–	–	–
Allocation Disagreement	8.8%	–	–	–	–	–	–	–	–	–	–

[a] Pixels in the Sparse Grass cover type were considered correct if the model predicted either Bare Ground or Grass.
[b] The accuracy of Unknown and Shadow were not included in error assessment.
[c] *Ephedra*, *Prosopis*, *Salsola*, *Yucca*, and Other Shrub counted as shrubs, and all other cover types except Shadow counted as non-shrubs.

data-rich sources of habitat information previously inaccessible to wildlife researchers and land managers. We estimated shrub and other vegetative cover at several sites in Chihuahuan Desert grasslands by using object-based, automated classification methods in the open-source Program R to convert UAS collected orthomosaic and elevation rasters into vegetation data layers (Fig. 5). Our efforts classified overall vegetative cover with accuracies of 77.2%–88.8% and shrub cover with accuracies between 95.7% and 99.2% across our four ecologically distinct study sites. The methods we developed (available at https://github.com/andy-bankert/GEOBIA-in-R) are some of the first to use open-source software for object-based classification on UAS-sourced data using Program R, and make this type of classification technique more accessible to ecologists wishing to use UAS as a tool for vegetation assessment in ecological study.

This work represents a significant step towards the development and implementation of flexible, low cost, open-source GEOBIA methods for UAS data over large study areas. Although some open-source software tools have been developed and successfully applied to multi–scale vegetation mapping and habitat classification (Clewley et al., 2014) as well as urban land use mapping (Grippa et al., 2017), the majority of grassland and shrubland vegetation classifications from UAS imagery have relied on proprietary software for image segmentation. While proprietary software can be more powerful, versatile, and efficient, we were still able to design a simple and low-cost alternative program that can incorporate the two most relevant parameters at our study sites (elevation thresholds and color similarity) into image segmentation and the resulting land cover classification maps. In future efforts, open-source flexibility could also extend to other program modifications including minor adjustments to threshold parameters, changing which features to analyze during segmentation and classification, specialized region-growing techniques, or significantly changing image segmentation and object classification methods.

Table 6
Confusion matrix showing the number of pixels in verified areas at the Marfa Grassland Priority Conservation Area in Texas, USA. Bold numbers refer to pixels where both the model and hand verification identified the same cover type. The accuracies reported show both the percentage of pixels assigned to the correct cover type and the percentage of pixels where the model correctly determined whether the pixel belonged to a shrub or a non-shrub.

	Bare Ground	Grass	*Salsola*	Other Shrub	*Yucca*	Sparse Grass[a]	Unknown[b]	Shadow[b]
Bare Ground	**9864**	48675	19	29	22	**83267**	317	232
Grass	2433	**177132**	72	207	84	**142888**	1489	1166
Salsola	0	39	**0**	1	0	142	0	6
Shadow	3	1679	0	96	33	1137	113	759
Other Shrub	0	162	7	**433**	123	207	179	110
Yucca	1	68	0	47	**418**	104	1	26
Producer Class Accuracy	80.2%	78.4%	0.0%	60.4%	64.6%	99.8%	–	–
Producer Shrub Accuracy[c]	100.0%	99.9%	92.9%	66.9%	83.6%	99.9%	–	–
User Class Accuracy	65.6%	99.1%	0.0%	46.5%	65.5%	–	–	–
User Shrub Accuracy[c]	100.0%	99.9%	99.5%	59.7%	72.9%	–	–	–
% Overall Correct Cover Type	88.8%	–	–	–	–	–	–	–
% Overall Correct Shrub Classification	99.8%	–	–	–	–	–	–	–
Quantity Disagreement	0.1%	–	–	–	–	–	–	–
Allocation Disagreement	0.2%	–	–	–	–	–	–	–

[a] Pixels in the Sparse Grass cover type were considered correct if the model predicted either Bare Ground or Grass.
[b] The accuracy of Unknown and Shadow not included in error assessment.
[c] Other Shrub, *Salsola*, and *Yucca* were considered shrubs, and all other cover types except Shadow counted as non-shrubs.

Table 7
Confusion matrix showing the number of pixels in verified areas at the Valle Colombia Grassland Priority Conservation Area in Coahuila, MX. Bold numbers refer to pixels where both the model and hand verification identified the same cover type. The accuracies reported show both the percentage of pixels assigned to the correct cover type and the percentage of pixels where the model correctly determined whether the pixel belonged to a shrub or a non-shrub.

	Hilaria	*Prosopis*	*Opuntia*	Other Shrub	Grass	Bare Ground	*Yucca*	Sparse Grass[a]	Unknown/Shadow[b]
Hilaria	**3452**	74	0	0	2167	170	0	5282	632
Prosopis	31	**1493**	55	1	2269	26	4	1155	2013
Opuntia	0	0	**0**	0	0	0	0	0	0
Other Shrub	0	0	0	**989**	158	33	1195	1297	1426
Grass	1161	1234	60	86	**111137**	7012	440	**124589**	8258
Bare Ground	436	109	14	10	27130	**18389**	52	**88960**	3193
Shadow	0	29	0	110	6	46	6	648	1247
Yucca	0	0	0	38	63	16	**3134**	689	383
Producer Class Accuracy	68.0%	51.3%	0.0%	88.0%	77.8%	71.7%	65.0%	96.2%	–
Producer Shrub Accuracy[c]	99.4%	51.3%	57.4%	91.5%	98.3%	99.7%	89.8%	98.6%	–
User Class Accuracy	31.0%	29.7%	–	26.9%	95.9%	79.5%	79.5%	–	–
User Shrub Accuracy[c]	99.3%	29.8%	–	59.5%	99.3%	99.9%	80.5%	–	–
% Overall Correct Cover Type	86.9%	–	–	–	–	–	–	–	–
% Overall Correct Shrub Classification	98.1%	–	–	–	–	–	–	–	–
Quantity Disagreement	2.7%	–	–	–	–	–	–	–	–
Allocation Disagreement	3.8%	–	–	–	–	–	–	–	–

[a] Pixels in the Sparse Grass cover type were considered correct if the model predicted either Bare Ground or Grass.
[b] The accuracy of Unknown and Shadow were not included in error assessment.
[c] *Prosopis*, Other Shrub, and *Yucca* counted as shrubs, and all other cover types except Shadow counted as non-shrubs.

While other hybrid approaches have used pixel-based results to inform object-based classification (Chen et al., 2017), ours is the first to use pixel-based methods to reclassify objects. This approach was uniquely suited for characterizing vegetation in this system because of the heterogeneous nature of grass and bare ground cover at the spatial scale of our pixels (0.02 m^2), not our objects (>0.06 m^2). Additionally, our use of several types of classification accuracies (i.e. overall classification accuracy, quantity and allocation disagreement, and object location accuracy) helped give context to traditional class-level accuracies derived from confusion matrices and is important to assess in desert landscapes. For example, *Dipodomys* mounds at the Chihuahua site had a 43% cover classification accuracy. However, our model successfully located most *Dipodomys* mounds by identifying at least some pixels correctly (object location accuracy) within a validation polygon 88% of the time. Similarly, *Prosopis* at the Coahuila site had a 51.3% cover classification accuracy, but an object location accuracy of 74%. Calculating allocation disagreement and object location accuracy as additional accuracy metrics gives information about the predicted presence or absence of a particular vegetative characteristic (e.g., vertical structure), which can be just as important to assess as the amount of vegetative cover on a landscape. For example, the presence of a single high point in an area can influence habitat use by sparrows (e.g. Marshall et al., 2020). Loggerhead shrikes (*Lanius* ludovicianus), a common predator of grassland birds, may utilize perches within their home ranges as vantage points to scan for prey (Macías-Duarte et al., 2018). The presence of a small number of shrubs in an area could therefore influence grassland bird populations in the area.

The methods we outline here are particularly promising for use in shrub removal and grassland improvement projects common in the Chihuahuan Desert. Shrub encroachment is one of the main drivers of regional grassland loss, and shrub cover is an important determinant of biomass (Cunliffe et al., 2020) as well as habitat quality and use for grassland wildlife (e.g. Macías-Duarte et al., 2018). These methods can be used as a tool for researchers and managers currently struggling to assess shrub cover at sites within desert grasslands. The use of UAS technology allows users to collect imagery as frequently as necessary, and during times of year and hours during the day ideal for data collection. For example, those wanting to measure the effects of herbicide treatment can use a UAS to collect imagery before and after treatment, and classify the collected imagery to quantify this change using the resulting data layers easier to interpret than ground-based measurements (Laliberte et al., 2004). Also, ecologists can pair UAS

Table 8
The number of objects from discrete cover types identified during verification at four Chihuahuan Desert study sites and the number of these objects where the model correctly located the object by identifying at least some of the object's pixels correctly. At the Chihuahua site, we identified objects during verification as well as randomly elsewhere across the study site for some cover types with few objects identified during verification and at all other sites we only used polygons digitized during verification.

		# of Objects Identified		Object Location
Site	Class	Hand Digitized	Computer	Accuracy
Durango	Other Shrub	47	44	93.6%
Durango	*Juniperus*	71	70	98.6%
Durango	*Brickellia*	80	51	63.8%
Chihuahua	*Dipodomys* mound[a]	110	97	88.2%
Chihuahua	*Prosopis*	76	72	94.7%
Chihuahua	*Yucca*	23	20	87.0%
Chihuahua	*Salsola*[a]	174	120	69.0%
Chihuahua	*Ephedra*[a]	161	95	59.0%
Chihuahua	*Pleuraphis*	95	67	70.5%
Texas	Other Shrub	26	19	73.1%
Texas	*Salsola*	2	0	0.0%
Texas	*Yucca*	26	22	84.6%
Coahuila	*Hilaria*	16	15	93.8%
Coahuila	*Prosopis*	77	57	74.0%
Coahuila	*Opuntia*	4	0	0.0%
Coahuila	Other Shrub	11	11	100.0%
Coahuila	*Yucca*	104	83	79.8%

[a] We identified *Dipodomys*, *Salsola*, and *Ephedra* objects outside of the verification tiles at the Chihuahua site to increase the number of verification objects.

Table 9
Oversegmentation factors of shrub classes at four study sites across the Chihuahuan Desert.

Site	Class	# Polygons	Average polygon area (m^2)	Oversegmentation factor (# objects per polygon)
Durango	*Brickellia*	423	1.41	6.7
Durango	*Juniperus*	378	16.51	28.2
Durango	Other Shrub	307	6.86	16.5
Durango	*Yucca*	38	1.01	6.0
Chihuahua	*Ephedra*	242	0.95	5.9
Chihuahua	*Prosopis*	127	13.00	40.4
Chihuahua	*Other Shrub*	150	0.97	4.2
Chihuahua	*Salsola*	213	2.30	10.4
Chihuahua	*Yucca*	188	0.93	5.6
Texas	*Salsola*	11	6.15	4.3
Texas	*Other Shrub*	191	1.52	3.7
Texas	*Yucca*	241	0.48	1.8
Coahuila	*Prosopis*	978	1.25	6.9
Coahuila	*Other Shrub*	189	3.58	19.4
Coahuila	*Yucca*	316	1.51	11.7

generated vegetation maps with GPS transmitter data to better understand how certain species interact with their habitat.

Future work in this area includes the improvement of our approach to map vegetation both in desert grasslands and other ecotypes. There are several opportunities for improved efficiency and accuracy in our classification methods, particularly in the image segmentation process. Eight of the total 26 cover types from the validation data had class-specific accuracies ≤60%, including *Brickellia*, *Opuntia*, *Salsola*, and *Ephedra*. This likely occurred because of the similarity of RGB spectral signatures between grass and these cover types (e.g. *Brickellia*, *Ephedra*, other shrubs at the Coahuila site, low growing sparse *Prosopis* at the

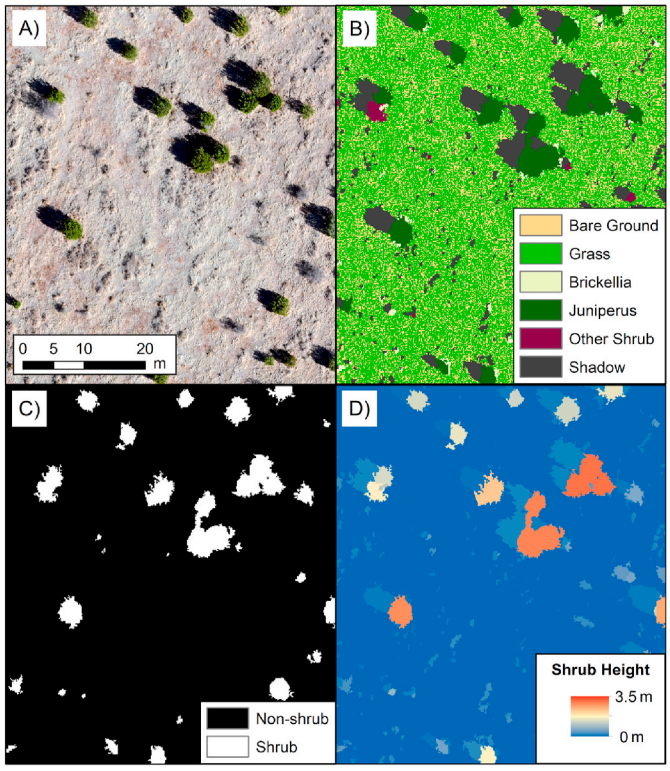

Fig. 5. An example of rasters showing A) Red Green Blue orthomosaic, B) vegetation cover classification, C) shrub presence/absence, and D) shrub height produced using UAS data layers and supervised random forest classification in desert grasslands. (For interpretation of the references to color in this figure legend, the reader is referred to the Web version of this article.)

Texas site, and *Salsola*; Appendix D), small training sample for uncommon cover types (i.e. *Salsola* in Texas [n = 11], *Opuntia* in Coahuila [n = 31]), and misclassification of a highway as bare ground at the Durango site, which appeared darker in the verification region than in the training region. Future efforts should prioritize training polygon collection for uncommon cover types that are ecologically important, spectrally similar cover types, or cover types with a very diverse signature to increase class-level accuracies. Collecting additional color bands, such as near infrared, and collecting imagery during the summer or fall before most shrubs have lost their leaves could help improve accuracy of classes with a similar spectral pattern to grass. Both of these methods require additional costs of either extra field time or extra flights and may not always be worth the benefit. Further, it is possible to improve upon the image segmentation work by incorporating different variables including intensity-hue-saturation and/or multispectral properties, as well as more complex algorithms such as edge detection, k-means clustering, and/or neural networks. Including additional features such as object texture, shape, and size could be useful for improving classification with improved image segmentation that correctly and completely delineates most objects. Our process only relied on one color threshold and two elevation thresholds to grow objects, and incorporating a variable threshold for color may have allowed the program to completely segment shrubs rather than oversegment them. Finally, as machine learning techniques advance, updated classification methods could be also employed to build upon the RF methods in our study.

12. Conclusions

UAS technology is a promising new tool for measuring vegetative cover across landscapes. We successfully used UAS collected imagery to create data layers of shrubs and other vegetative cover in grasslands of

the Chihuahuan Desert and generated high-accuracy vegetation layers for our study sites to understand habitat use in deserts grassland species wintering in these areas. Our methods can be used in other sites in desert grasslands to measure shrub cover at time intervals and spatial extent specific to a study and have particular potential for use in shrub removal studies to directly measure change in shrub cover before and after treatment. Our work is some of the first to use the open-source software Program R to build land cover datasets from UAS-generated orthomosaic and elevation rasters using object-based methods. Given the flexible nature of these methods, our approaches can also be modified for use outside of grasslands in other systems and settings. Ideally our work can serve as a foundation upon which future researchers can build to customize the classification process to answer questions ecologically relevant to a broad range of habitats.

CRediT authorship contribution statement

Andrew R. Bankert: Methodology, Software, Validation, Formal analysis, Data curation, Writing - original draft, Writing - review & editing, Visualization. **Erin H. Strasser:** Conceptualization, Investigation, Data curation, Writing - review & editing, Project administration, Funding acquisition. **Cristy G. Burch:** Methodology, Investigation, Resources, Writing - review & editing. **Maureen D. Correll:** Conceptualization, Investigation, Resources, Data curation, Writing - original draft, Visualization, Supervision, Project administration, Funding acquisition.

Declaration of competing interest

The authors declare that they have no known competing financial interests or personal relationships that could have appeared to influence the work reported in this paper.

Equation (1). Formula for Euclidian distance (d_{Euclid}) using the Red, Green, and Blue values for both seed and test pixels.

$$d_{Euclid} = \sqrt{\left((Red_{seed} - Red_{test})^2 + (Green_{seed} - Green_{test})^2 + (Blue_{seed} - Blue_{test})^2\right)} \quad (1)$$

Acknowledgements

This work was funded by The US Fish and Wildlife Service Neotropical Migratory Bird Conservation Act (award #F18AP00633 and F19P00607) the Canadian Wildlife Service, Alianza WWF-Fundación Carlos Slim, The Bobolink Foundation, and the US Forest Service International Program. We thank landowners and managers of the field sites for providing access and logistical support. This includes Fondo Mexicano para la Conservación de la Naturaleza and The Nature Conservancy for Rancho El Uno (Chihuahua site), The Dixon Water Foundation for Mimm's Ranch (Texas site), O Bermudez Finnan for Rancho Valle Colombia (Coahuila site), and G Bredeé Ortiz and I Gariá Bredee for Rancho Santa Teresa and Rancho El Regalo (the Durango site) respectively. We also thank PML Serrano for help in initial UAS flight planning, A Shaw for support in UAS image processing, and TB Ryder for review of an earlier version of the manuscript that greatly improved its content. The views and opinions expressed here are those of the authors and do not necessarily reflect the position of our funders.

Appendix A. Supplementary data

Supplementary data to this article can be found online at https://doi.org/10.1016/j.jaridenv.2020.104383.

References

Anadón, J.D., Sala, O.E., Turner, B.L., Bennett, E.M., 2014. Effect of woody-plant encroachment on livestock production in North and South America. Proc. Natl. Acad. Sci. Unit. States Am. 111, 12948–12953. https://doi.org/10.1073/pnas.1320585111.

Anderson, K., Gaston, K.J., 2013. Lightweight unmanned aerial vehicles will revolutionize spatial ecology. Front. Ecol. Environ. 11, 138–146. https://doi.org/10.1890/120150.

Báez, S., Collins, S.L., 2008. Shrub invasion decreases diversity and alters community stability in northern Chihuahuan Desert plant communities. PLoS One 3. https://doi.org/10.1371/journal.pone.0002332.

Bestelmeyer, B.T., Peters, D.P., Archer, S.R., Browning, D.M., Okin, G.S., Schooley, R.L., Webb, N.P., 2018. The grassland–shrubland regime shift in the southwestern United States: misconceptions and their implications for management. Bioscience 68, 678–690. https://doi.org/10.1093/biosci/biy065.

Blaschke, T., Burnett, C., Pekkarinen, A., 2004. Image segmentation methods for object-based analysis and classification. In: de Jong, S.M., van der Meer, F.D. (Eds.), Remote Sensing Image Analysis: Including the Spatial Domain. Springer, Dordrecht, pp. 211–236.

Blaschke, T., 2010. Object based image analysis for remote sensing. ISPRS J. Photogrammetry Remote Sens. 65, 2–16. https://doi.org/10.1016/j.isprsjprs.2009.06.004.

Blaschke, T., Hay, G.J., Kelly, M., Lang, S., Hofmann, P., Addink, E., Queiroz Feitosa, R., van der Meer, F., van der Werff, H., van Coillie, F., Tiede, D., 2014. Geographic object-based image analysis - towards a new paradigm. ISPRS J. Photogrammetry Remote Sens. 87, 180–191. https://doi.org/10.1016/j.isprsjprs.2013.09.014.

Chen, Z., Pasher, J., Duffe, J., Behnamian, A., 2017. Mapping arctic coastal ecosystems with high resolution optical satellite imagery using a hybrid classification approach. Can. J. Rem. Sens. 43, 513–527. https://doi.org/10.1080/07038992.2017.1370367.

Chen, G., Weng, Q., Hay, G.J., He, Y., 2018. Geographic object-based image analysis (GEOBIA): emerging trends and future opportunities. GIScience Remote Sens. 55, 159–182. https://doi.org/10.1080/15481603.2018.1426092.

Clewley, D., Bunting, P., Shepherd, J., Gillingham, S., Flood, N., Dymond, J., Lucas, R., Armston, J., Moghaddam, M., 2014. A python-based open source system for Geographic Object-Based Image Analysis (GEOBIA) utilizing raster attribute tables. Rem. Sens. 6, 6111–6135. https://doi.org/10.3390/rs6076111.

Cunliffe, A.M., Brazier, R.E., Anderson, K., 2016. Ultra-fine grain landscape-scale quantification of dryland vegetation structure with drone-acquired structure-from-motion photogrammetry. Remote Sens. Environ. 183, 129–143. https://doi.org/10.1016/j.rse.2016.05.019.

Cunliffe, A.M., McIntire, C.D., Boschetti, F., Sauer, K.J., Litvak, M., Anderson, K., Brazier, R.E., 2020. Allometric relationships for predicting aboveground biomass and sapwood area of Oneseed Juniper (Juniperus monosperma) trees. Front. Plant Sci. 11, 94. https://doi.org/10.3389/fpls.2020.00094.

Dong, Y., Yan, H., Wang, N., Huang, M., Hu, Y., 2019. Automatic identification of shrub-encroached grassland in the Mongolian plateau based on UAS remote sensing. Rem. Sens. 11, 1–22.

Deluca, G., Silva, J.M.N., Cerasoli, S., Araujo, J., Campos, J., Di Fazio, S., Modica, G., 2019. Object-based land cover classification of cork oak woodlands using UAV imagery and Orfeo Toolbox. Rem. Sens. 11, 2–22. https://doi.org/10.3390/rs11101238.

Fuller, R.M., Groom, G.B., Jones, A.R., 1994. The land cover map of Great Britain: an automated classification of Landsat thematic mapper data. Photogramm. Eng. Rem. Sens. 60, 553–562.

Glisson, W.J., Brady, R.S., Paulios, A.T., Jacobi, S.K., Larkin, D.J., 2015. Sensitivity of secretive marsh birds to vegetation condition in natural and restored wetlands in Wisconsin. J. Wildl. Manag. 79, 1101–1116. https://doi.org/10.1002/jwmg.937.

Godínez-Alvarez, H., Herrick, J.E., Mattocks, M., Toledo, D., Van Zee, J., 2009. Comparison of three vegetation monitoring methods: their relative utility for ecological assessment and monitoring. Ecol. Indicat. 9, 1001–1008. https://doi.org/10.1016/j.ecolind.2008.11.011.

Grippa, T., Lennert, M., Beaumont, B., Vanhuysse, S., Stephenne, N., Wolff, E., 2017. An open-source semi-automated processing chain for urban object-based classification. Rem. Sens. 9, 358. https://doi.org/10.3390/rs9040358.

Halstead, B.J., Thompson, M.E., Amarello, M., Smith, J.J., Wylie, G.D., Routman, E.J., Casazza, M.L., 2019. Effects of prescribed fire on San Francisco gartersnake survival and movement. J. Wildl. Manag. 83, 231–240. https://doi.org/10.1002/jwmg.21585.

Hassler, S.C., Baysal-Gural, F., 2019. Unmanned Aircraft System (UAS) technology and applications in agriculture. Agronomy 9, 1–21. https://doi.org/10.3390/agronomy9100618.

Hay, G.J., Castilla, G., 2008. Geographic object-based image analysis (GEOBIA): a new name for a new discipline. Lect. Notes Geoinf. Cartogr. 75–89. https://doi.org/10.1007/978-3-540-77058-9_4.

Horn, B.K., 1981. Hill shading and the reflectance map. Proc. IEEE 69, 14–47.

Huenneke, L.F., Clason, D., Muldavin, E., 2001. Spatial heterogeneity in Chihuahuan Desert vegetation: implications for sampling methods in semi-arid ecosystems. J. Arid Environ. 47, 257–270. https://doi.org/10.1006/jare.2000.0678.

Hunt, K.L., Fraser, J.D., Friedrich, M.J., Karpanty, S.M., Catlin, D.H., 2018. Demographic response of Piping Plovers suggests that engineered habitat restoration is no match for natural riverine processes. Condor 120, 149–165. https://doi.org/10.1650/condor-17-93.1.

Hussain, M., Chen, D., Cheng, A., Wei, H., Stanley, D., 2013. Change detection from remotely sensed images: from pixel-based to object-based approaches. ISPRS J.

Photogrammetry Remote Sens. 80, 91–106. https://doi.org/10.1016/j.isprsjprs.2013.03.006.

Jacques, C.N., Jenks, J.A., Grovenburg, T.W., Klaver, R.W., 2015. Influence of habitat and intrinsic characteristics on survival of neonatal pronghorn. PloS One 10. https://doi.org/10.1371/journal.pone.0144026.

Lai, J., Lortie, C.J., Muenchen, R.A., Yang, J., Ma, K., 2019. Evaluating the popularity of R in ecology. Ecosphere 10, 1–7. http://onlinelibrary.wiley.com/doi/10.1002/ecs2.2567/full.

Laliberte, A.S., Rango, A., Havstad, K.M., Paris, J.F., Beck, R.F., McNeely, R., Gonzalez, A.L., 2004. Object-oriented image analysis for mapping shrub encroachment from 1937 to 2003 in southern New Mexico. Remote Sens. Environ. 93, 198–210. https://doi.org/10.1016/j.rse.2004.07.011.

Laliberte, A., Rango, A., 2011. Image processing and classification procedures for analysis of sub-decimeter imagery acquired with an unmanned aircraft over arid rangelands. GIScience Remote Sens. 48, 4–23. https://doi.org/10.2747/1548-1603.48.1.4.

Li, M., Lei, M., Blashcke, T., Cheng, L., Tiede, D., 2016. A systematic comparison of different object-based classification techniques using high spatial resolution imagery in agricultural environments. Int. J. Appl. Earth Obs. Geoinf. 47, 87–98. https://doi.org/10.1016/j.jag.2016.01.011 0303-2434.

Liaw, A., Wiener, M., 2002. Classification and regression by randomForest. R. News 2, 18–22.

Lu, B., He, Y., Liu, H., 2016. 4th International Workshop on Earth Observation and Remote Sensing Applications (EORSA). 107-111. In: Investigating Species Composition in a Temperate Grassland Using Unmanned Aerial Vehicle-Acquired Imagery. IEEE. https://doi.org/10.1109/EORSA.2016.7552776.

Ma, L., Li, M., Ma, X., Cheng, L., Du, P., Liu, Y., 2017. A review of supervised object-based land-cover image classification. ISPRS J. Photogrammetry Remote Sens. 130, 277–293. https://doi.org/10.1016/j.isprsjprs.2017.06.001.

Macías-Duarte, A., Panjabi, A.O., Pool, D.B., Ruvalcaba-Ortega, I., Levandoski, G.J., 2018. Fall vegetative cover and summer precipitation predict abundance of wintering grassland birds across the Chihuahuan desert. J. Arid Environ. 156, 41–49. https://doi.org/10.1016/j.jaridenv.2018.04.007.

Marsett, R.C., Qi, J., Heilman, P., Biedenbender, S.H., Watson, M.C., Amer, S., Marsett, R., 2006. Remote sensing for grassland management in the arid southwest. Rangel. Ecol. Manag. 59, 530–540. https://doi.org/10.2111/05-201R.1.

Marshall, H., Blomberg, E.J., Watson, V., Conway, M., Cohen, J.B., Correll, M.D., Elphick, C.S., Hodgman, T.P., Kovach, A.I., Shriver, W.G., Wiest, W.A., Olsen, B.J., 2020. Horizon angle and edge avoidance predict saltmarsh sparrow abundance better than habitat area. Condor 122 (3).

Meyer, G.E., Von Bargen, K., Woebbecke, D.M., Mortensen, D.A., 1994. Shape Features for Identifying Young Weeds Using Image Analysis. American Society of Agricultural Engineers.

Montandon, L.M., Small, E.E., 2008. The impact of soil reflectance on the quantification of the green vegetation fraction from NDVI. Rem. Sens. Environ. 112, 1835–1845. https://doi.org/10.1016/j.rse.2007.09.007.

Pajares, G., 2015. Overview and current status of remote sensing applications based on unmanned aerial vehicles (UAVs). Photogramm. Eng. Rem. Sens. 81, 281–329. https://doi.org/10.14358/PERS.81.4.281.

Polley, H.W., Johnson, H.B., Tischler, C.R., 2003. Woody invasion of grasslands: evidence that CO 2 enrichment indirectly promotes establishment of Prosopis glandulosa. Plant Ecol. 164, 85–94.

Pontius Jr., R.G., Millones, M., 2011. Death to Kappa: birth of quantity disagreement and allocation disagreement for accuracy assessment. Int. J. Rem. Sens. 32, 4407–4429. https://doi.org/10.1080/01431161.2011.552923.

Rampant, R., Zdunic, K., Burrows, N., 2019. UAS and Landsat imagery to determine fuel condition for fire behaviour prediction on spinifex hummock grasslands of arid Australia. Int. J. Rem. Sens. 40, 9126–9139.

Robertson, L.D., King, D.J., 2011. Comparison of pixel-and object-based classification in land cover change mapping. Int. J. Rem. Sens. 32, 1505–1529. https://doi.org/10.1080/01431160903571791.

Rosenberg, K.V., Dokter, A.M., Blancher, P.J., Sauer, J.R., Smith, A.C., Smith, P.A., Stanton, J.C., Panjabi, A., Helft, L., Parr, M., Marra, P.P., 2019. Decline of the north American avifauna. Science 366, 120–124. https://doi.org/10.1126/science.aaw1313.

Shaffer, J.A., DeLong, J.P., 2019. The effects of management practices on grassland birds—an introduction to North American grasslands and the practices used to manage grasslands and grassland birds. Prof. Pap. 74 https://doi.org/10.3133/pp1842A.

Teodoro, A.C., Araujo, R., 2016. Comparison of performance of object-based image analysis techniques available in open source software (Spring and Orfeo Toolbox/Monteverdi) considering very high spatial resolution data. J. Appl. Remote Sens. 10, 016011. https://doi-org.wv-o-ursus-proxy02.ursus.maine.edu/10.1117/1.JRS.10.016011.

U.S. Geological Survey, 2016. Landsat—Earth observation satellites (ver. 1.2, April 2020): U.S. Geological Survey Fact Sheet 2015–3081. https://doi.org/10.3133/fs20153081.

Yang, X., Guo, X., 2014. Quantifying responses of spectral vegetation indices to dead materials in mixed grasslands. Rem. Sens. 6, 4289–4304. https://doi.org/10.3390/rs6054289.

Zhang, H., Sun, Y., Chang, L., Qin, Yu, Chen, J., Qin, Yan, Du, J., Yi, S., Wang, Y., 2018a. Estimation of grassland canopy height and aboveground biomass at the quadrat scale using unmanned aerial vehicle. Rem. Sens. 10 https://doi.org/10.3390/rs10060851.

Zhang, Z., Gerke, M., Vosselman, G., Yang, M., 2018b. Filtering Photogrammatic point clouds using standard lidar filters towards DTM generation. ISPRS Ann. Photogram., Rem. Sens., Spatial Informat. Sci. IV, 4–7. https://doi.org/10.5194/isprs-annals-IV-2-319-2018.